Journal Name

ARTICLE

Construction of structural diversity and fine-tuned porosity in acylamide MOFs by synthetical approach

Wan-Ting Yao, Ming-Biao Luo, Xue-Feng Feng*, Pan-Pan Meng, Le-Le Gong, and Feng Luo*

Four new metal-organic frameworks (MOFs), namely $Zn(L1)(AzDC)\cdot(DMF)_3$ (**1**), $Zn(L2)(AzDC)\cdot(DMF)_{0.5}(H_2O)$ (**2**), $Zn_2(AzDC)_2(L3)\cdot(DMF)(H_2O)_{0.5}$(**3**), $Zn(AzDC)(L3)\cdot(DMF)$(**4**), (L1=N^1,N^4-di(pyridin-4-yl)terephthalamide, L2=N^1,N^4-di(pyridin-3-yl)terephthalamide, L3=$N^4,N^{4'}$- di(pyridin-4-yl)-[1,1'-biphenyl]-4,4'-dicar-boxamide, H_2AzDC=4,4'-(diazene-1,2-diyl)dibenzoic acid, DMF=N,N-dimethylformamide), were prepared by the solvothermal reaction of $Zn(NO_3)_2$, H_2AzDC, and acylamide ligands. Polymers **1-3** show the common layer-pillared **pcu**-type net with four- or two-fold interpenetration, while polymer **4** displays an unprecedented four-connected net with 6^38^210 topology symbol. Note that the difference in the pillar like that of L1 for **1** and L2 for **2** in a manner of position isomer caused significant alteration involving in interpenetration number from four to two, enhanced potential porosity from 47.1% to 66.6%, as well as pore configuration from smaller triangle window to bigger quadrangle window. Furthermore, controlling the magnitude of reaction solvent like that of 5 mL for **3** and 15 mL for **4** resulted also significant alteration involving in structural diversity from four-fold interpenetrating **pcu** net to two-fold interpenetrating 6^38^210 net, enhanced potential porosity from 49.1% to 57.2%, as well as pore configuration from smaller rectangle window to bigger quadrangle window. Most importantly, all these polymers display highly selective adsorption of CO_2 over other gases like that of N_2, CH_4, CO, and O_2, most likely, due to the free standing acylamide groups in them that afford unique affinity towards CO_2.

Introduction

The design and synthesis of metal-organic frameworks (MOFs) have drawn a large amount of attention since 1960s owing to their diverse architectures and a range of potential applications in many fields, such as luminescence, catalysis, gas absorption, separation, ion exchange and magnetism.[1-3] However, the rational design and controlled synthesis are still challenging topics as their formations are based on the interplay of starting materials, pH value, template, reaction temperature, solvent, reagent concentration metal-to-ligand ratio.[4-7] There is no doubt that the rational synthesis of such materials are more unpredictable and further systematic studies by controlling diversified conditions are important of great interest. For example, there have made many efforts to control interpenetration of identical nets to enhance porosity. Yaghi and co-workers have shown how the interpenetration can be controlled by high dilution of solution.[8] By taking full advantage of template reagents, a so-called template effect, has been developed by Kitagawa, Zhu, Lin and co-workers to control interpenetration and modulate porosity.[9] To determining what is the dominating fact capable of controlling interpenetration of nets, a systematic investigation on synthetic conditions was explored by Zaworotko and co-workers, revealing

that at least in their case interpenetration is controlled by both temperature and concentration.[10] Likewise, as stated by Xu and co-workers, interpenetration and continuous porosity are controlled by both temperature and concentration among three isomers, where two isomers are associated with reaction temperature, whereas the other two isomers are govern by concentration of solution.[11] Moreover, like liquid-phase epitaxial growth reported by Shekhah and co-workers,[12] rational design of organic ligands attested by Hupp and co-workers,[13] these elegant methods have also been developed for such purpose. Besides, in some cases solvent-induced supramolecular isomers, pH-caused supramolecular isomers, pH dependent crystallization of chirality, temperature-controlled structural diversity, and so on, were also observed.[14] In this work, we report some interesting results in this category, and the synthesis, structure, characterization of four new MOFs in detail.

Experimental Section

Synthesis.

Synthesis of $Zn(L1)(AzDC)\cdot(DMF)_3$ (1). A mixture of $Zn(NO_3)_2$ (0.2mmol), H_2AzDC(0.2mmol), and L1(0.2mmol) in DMF (5mL) was sealed in a Teflon-lined stainless steel vessel and heated at 115ºC for 3 days, and then the reaction system was cooled to room temperature. Red crystals were obtained. Yield: 65% based on Zn. Elemental analysis (%): Calc.: C 54.83, H 4.27, N 12.79. Found: C 54.64, H 4.57, N 12.58.

$Zn(L2)(AzDC)\cdot(DMF)_{0.5}(H_2O)$ (2). A mixture of $Zn(NO_3)_2$ (0.2mmol), H_2AzDC(0.2mmol), and L2(0.2mmol) in DMF (5mL) was sealed in a Teflon-lined stainless steel vessel and heated at 115ºC for 3 days, and then the reaction system was cooled to room

School of Biology, Chemistry and Material Science, East China University of Technology, Nanchang, Jiangxi 344000, China, xffeng@ecit.cn and ecitluofeng@163.com

temperature. Red crystals were obtained. Yield: 73% based on Zn. Elemental analysis (%): Calc.: C 55.86, H 3.60, N 11.54. Found: C 53.55, H 3.42, N 11.37.

$Zn_2(AzDC)_2(L3)\cdot(DMF)(H_2O)_{0.5}(3)$. A mixture of $Zn(NO_3)_2\cdot6H_2O$ (0.2 mmol), H_2AzDC (0.2 mmol) and L (0.2 mmol) in DMF (5 ml) was sealed in a Teflon reactor and heated at 115˚C for 3 days, and then cooled to room temperature at 3˚C/h. Subsequently, red block crystals were obtained in 70% yield based on Zn. Element analysis (%) for **3**: calc: C 58.42, H 3.37, N 10.66; found: C 58.29, H 3.51, N 10.43.

$Zn(AzDC)(L3)\cdot(DMF)(4)$. A mixture of $Zn(NO_3)_2\cdot6H_2O$ (0.2 mmol), H_2AzDC (0.2 mmol) and L (0.2 mmol) in DMF (15 ml) in a ratio of 1:1:1 was sealed in a Teflon reactor, and heated at 115˚C for 3 days, and then cooled to room temperature at 3˚C/h. Subsequently, orange slice crystals were obtained in 50% yield based on Zn. Element analysis (%) for **4**: calc: C 62.65, H 3.77, N 11.31; found: C 62.45, H 3.54, N 11.13.

Materials and General Methods. All chemicals and solvents used in the syntheses were of analytical grade and used without further purification. The acylamide ligands were synthesized according to the method of literature. Thermogravimetric analysis (TGA) was performed by a TGA Q500 thermal analysis system. All TGA experiments were performed under a N_2 atmosphere from 40-800°C at a rate of 5°C /min. Data were analyzed using the TA Universal Analysis software package. X-ray powder diffraction were collected by a Bruker AXS D8 Discover powder diffractometer at 40 kV, 40 mA for Cu Kα, (λ = 1.5406Å). The simulated powder patterns were calculated by Mercury 1.4. The purity of the bulk products were determined by comparison of the simulated and experimental PXRD patterns. The as-synthesized sample (weight of about 100 mg) was degassed in the sample tube and dried for 24 h at 200 °C prior to measurements. Ultrahigh-purity-grade (> 99.999%) N_2, CO, O_2, CO_2, and CH_4 gases were used in this adsorption measurement. To maintain the experimental temperatures liquid nitrogen (77 K), temperature-programmed water bath (273 and 293 K) were used respectively.

X-ray Crystallography. Unit cell measurements and intensity data were collected at 113 K on a Bruker-AXS SMART Breeze CCD diffractometer using graphite monochromated MoKα radiation (λ=0.71073 Å). The data reduction included a correction for Lorentz and polarization effects, with an applied multi-scan absorption correction (SADABS). The crystal structure was solved and refined using the SHELXTL program suite. Direct methods yielded all non-hydrogen atoms, which were refined with anisotropic thermal parameters. All hydrogen atom positions were calculated geometrically and were riding on their respective atoms. The solvent molecules were treated by Platon Squeeze program. CCDC numbers are 1409106-1409107 for polymers **1-2**, and 1414037-1414038 for polymers **3-4**. The data can be obtained free of charge (http://www.ccdc.cam.ac.uk/data_request/cif).

Results and Discussion

Crystal Structure. The coordination mode of carboxylate ligands and the conformation of acylamide ligands in polymers **1-4** are shown in Scheme 1.

Single-crystal X-ray diffraction analysis shows that **1** crystallizes in the monoclinic *C2/c* space group. The Zn(II) ions show a common paddle-wheel, $Zn_2(O_2C)_4$ subunit and coordination site on the axis orientation is occupied by L1 nitrogen atoms. The $Zn_2(O_2C)_4$ subunits through carboxylate ligand ($AzDC^{2-}$) generate a 2D layer, then which is further supported by long nitrogen ligands (L1). The span between two adjacent layers is almost close to 2 nm, while the size of the 4^4 layer is ca. $17.2\times17.2Å^2$, indicative of big, potential porous framework. However, this will further undergo four-fold interpenetration, thus only affording smaller, trigonal channel along *c* axis and 47.1% solvent-accessible volume (Fig. 1d).[15]

By contrast, when position isomer of L2 is used, although this also generates the paddle-wheel, $Zn_2(O_2C)_4$ subunit and finally layer-pillared framework, however, several distinct characters are observed in the aspects of interpenetration, pore structure, and potential porosity. In contrast to polymer **1**, the degree of interpenetration is effectively reduced, only giving two-fold interpenetration in polymer **2**. Corresponding to this is the big quadrangular channel along *c* axis and enhanced solvent-accessible volume of 66.6% (Fig. 1h).[15]

To deep understand this feature, we select the smallest cuboid box to make a careful analysis (Fig. 1b, f). The 4^4 grid of layer in both **1** and **2** is constructed by $Zn_2(O_2C)_4$ subunit and $AzDC^{2-}$ linkers (Fig. 1a, e), thus, resulting in window of ca. $17.2\times17.2Å^2$. But slight difference could be found in the aspects of distortion between two phenyl groups of $AzDC^{2-}$ ligand. In **1** this is not observed, whereas in **2** partial $AzDC^{2-}$ ligands undergo this distortion, giving a dihedral angel of ca. 25°. However, we do not think this kind of factor could cause the significant change in interpenetration, pore structure, and potential porosity between **1** and **2**. Then we focus on the pillar of position isomers. Fig. 1 clearly depicts the difference of the configuration of the smallest box (Fig. 1b, f), where polymer **1** shows a regular box with the length of 2 nm (approximately equal to the length of L1 ligand) and the angle of approximately 90°, whereas a slantwise box is observed in polymer **2** and accompanied is the decrease of length (1.7 nm) and significant incline with angle of 56°. This directly causes one of the faces of this slantwise box to become cabined and less accessible. Thereby, we think this should be responsible for the decrease of interpenetration number for polymer **2** when a position isomer is utilized as pillars.
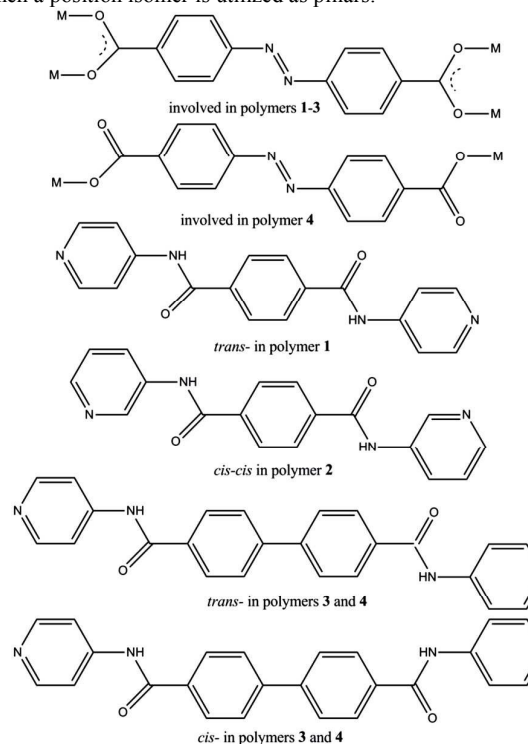
Scheme 1. Schematic description of the coordination mode of $AzDC^{2-}$ carboxylate ligands and the conformation of acylamide ligands in polymers **1-4**. The *trans* conformation in polymers **1**, **3**, **4** means that the two C=O units of acylamide ligands locate in the opposite side, while *cis* conformation in polymers **3**, **4** means that the two C=O units of acylamide ligands locate in the same side. As for the *cis-cis* conformation in polymer **2**, each *cis* means that the pyridine nitrogen atom and C=O unit of acylamide locate in the same side.

Journal Name

ARTICLE
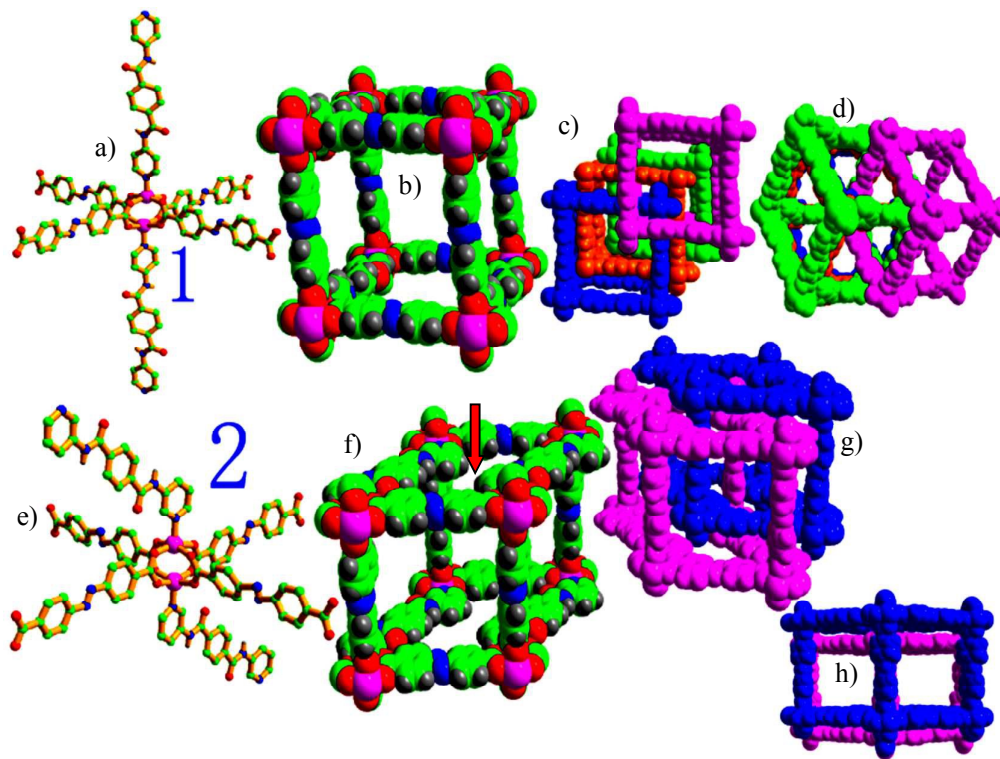
Fig. 1 A structural comparison between **1** and **2** involving in the a), e) paddle-wheel, $Zn_2(O_2C)_4$ subunit plus pillars of position isomers, b), f) the smallest box, c), g) the interpenetration of identical boxes, as well as d), h) the pore configuration of them with the aperture of 3.5 Å for **1** and 10.3Å for **2**. The face pointing by arrowhead presents the contractive face in **2**.

As show in Fig. 2, the single X-ray crystal structure reveals that **3** crystallizes in the monoclinic space group C2/c, and its asymmetric unit includes two crystallography-independent Zn(II) ions, two L3 and four AzDC^{2-} ligands. Each Zn(II) site is five-coordinated in a regular pyramidal geometry by four oxygen atoms (Zn1-O4/2.039(8), Zn1-O6/2.030(8), Zn1-O8/2.030(7), Zn1-O10/2.042(8), Zn2-O3/1.982(9), Zn2-O5/1.947(11), Zn2-O7/2.009(10), Zn2-O9/1.991(11) Å) from four AzDC^{2-} and one nitrogen atom (Zn1-N1/1.915(8), Zn2-N4/2.006(15) Å) from one L3 ligand. The AzDC^{2-} ligand adopts the bi(bidentate) mode and takes the μ_4-η^1:η^1:η^1:η^1 coordination mode while L3 ligand connects to two Zn(II) ions by its pyridyl nitrogen atom. Typically, binuclear Zn(II) ions are combined together by four carboxyl groups from four AzDC^{2-} ligands, generating the common paddle-wheel $\{Zn_2(O_2C)_4\}$ unit. Within *ab* plane, through AzDC^{2-} connectors these $\{Zn_2(O_2C)_4\}$ units forms a 2D layer. And this is further extended by L3 ligands to generate an overall 3D layer-pillared net. Generally speaking, this kind of net could be simplified to be a six-connected **pcu** net, based on the consideration of each $\{Zn_2(O_2C)_4\}$ unit acting as six-connecting node. Note that, regardless of four-fold interpenetration, considerable solvent-accessible volume,

equal to 49.1% of cell volume, estimated by Platon, is observed in **3**.[15]
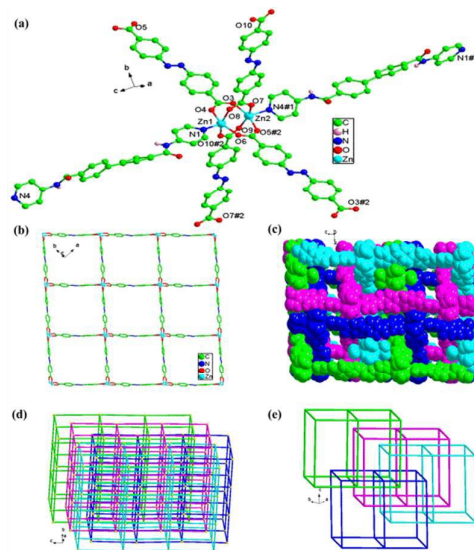
Fig. 2 (a) The symmetrical unit of **3** and the coordination environment of Zn(II) in it**.** The hydrogen atoms are omitted for clarity. Color code: Zn/blue-green, C/green, N/blue, O/red; (b) View of the 2D network of it; (c) The porous framework of **3** with the aperture of 3.8 Å; (d) Schematic description of the six-connected **pcu** net with four-fold interpenetration; (e) View of the interpenetrating mode in the four-fold interpenetrating net (each color represents one identical net).
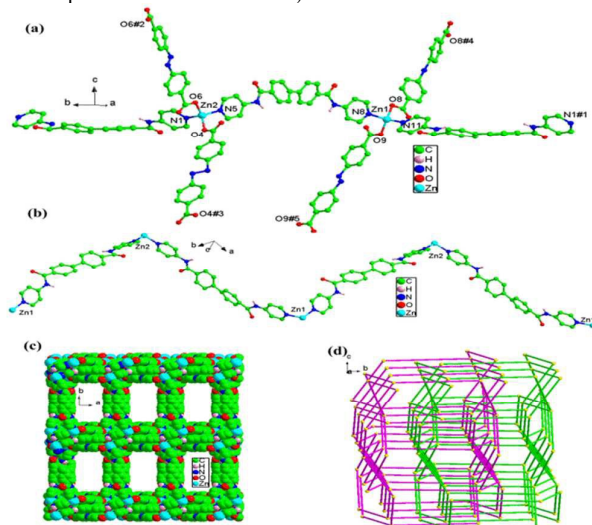
Fig. 3 (a) The symmetrical unit of **4** and the coordination surrounding around Zn(II) ion. Color code: Zn/blue-green, C/green, N/blue, O/red; (b) View of the 1D chain structure**;** (c) The porous framework in **4** with the aperture of 6.4 Å; (d) The 4-connected $6^3 8^2 10$ topology net with two-fold interpenetration.

The framework of **4** is very different from **3** and the asymmetric unit includes two crystallography-independent Zn(II) ions, three L3 ligands and four $AzDC^{2-}$ ligands. As show in Fig. 3, both Zn1 and Zn2 are four-coordinated with distorted tetrahedral geometry finished by oxygen atoms (Zn1-O8/1.986(12), Zn1-O9/1.947(8), Zn2-O4/1.901(11), Zn2-O6/1.946(12) Å) from $AzDC^{2-}$ ligands and nitrogen atoms (Zn1-N8/2.033(14), Zn1-N11/2.016(6), Zn2-N1/1.997(12), Zn2-N5/1.997(17) Å) from L ligands. The $AzDC^{2-}$ ligand adopts the bi(monodentate) mode and takes the $\mu_2:\eta^1:\eta^0:\eta^1:\eta^0$ coordination mode. L3 ligands connect to Zn1 and Zn2, forming a 1D chain. Furthermore, the combination of 1D chains and $AzDC^{2-}$ creates overall 3D framework, allowing for two-fold interpenetration. But, considerable solvent-accessible void is observed, which is estimated by Platon, giving 57.2% of the cell volume.[15] Topology analysis by Topos40 program gives an unprecedented 4-connected topology net with $6^3 8^2 10$ symbol.[16]

Thermostability and Gas Adsorption. The thermostability of them is explored by TG studies at 30-800°C (Fig. 4). For **1**, the first weight loss before 200°C is 18.2%, equal to three DMF molecules (18.6%), whereas for **2** the first weight loss should be the removal of half of DMF plus one water molecule (exp. 10.0%, calc. 10.6%) before 300°C. Sample **3** shows the first weight loss of 5.3%(calc. 5.3%) observed in the temperature range of 30-250℃, due to the removal of guest molecules of one DMF molecule and half of H_2O molecule. Sample **4** loses 10.0% (calc. 10.2%) at the first step from 30-250℃, which is equivalent to four DMF molecules.

Before carrying out gas adsorption, the as-synthesized samples of them are pretreated by immerging in CH_3OH for three days and then degassed under vacuum at 150°C for 24h. TG is further used to trace the degassing process. It is clear that in the activated samples of **1**-**4** solvent molecules were completely removed after

degassing treatment. The thermostability of MOF skeleton of them was estimated by PXRD investigations. As shown in Fig. S1, we can conclude that the fresh samples of them can maintain the crystalline state. And this can be also retained in polymers **1** and **4** even after activating at 150°C, but polymers **2** and **3** seems losing crystalline state badly and polymer **2** even became somewhat amorphous state.
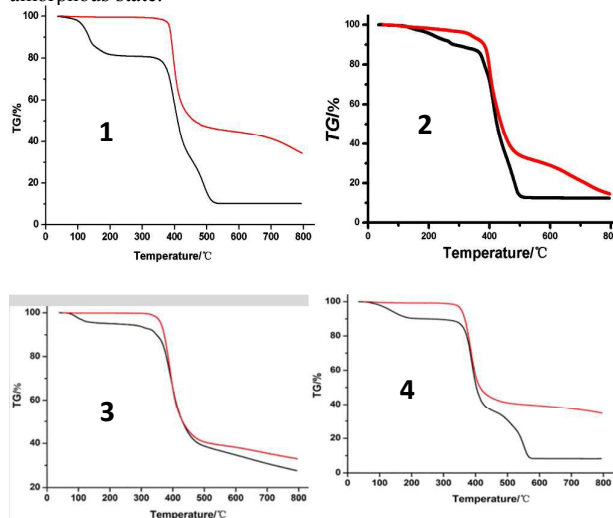
Fig. 4 The TG plots of polymers **1**-**4** for the as-synthesized samples and that after 150°C activation.

Furthermore, the porosity is investigated by gas adsorption studies. Both 77K and 293K N_2 adsorption for polymer **1** and **2** suggests almost no N_2 adsorption, mainly because of formation of amorphous state after activation in polymer **2** (as evidenced by PXRD investigations) and aperture of 3.5Å in polymer **1** less than the diameter of N_2 molecule of 3.64Å (Fig. S2).
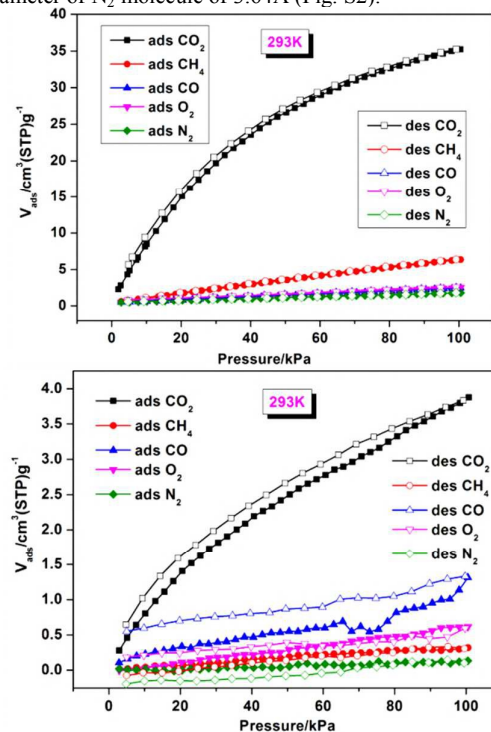
Fig. 5 Gas adsorption isotherms of **1**/right and**2**/left for CO_2, N_2, O_2, and CO at 293K.
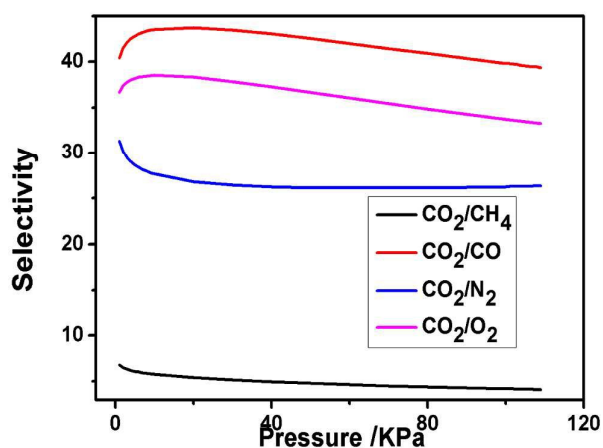
Fig. 6 The calculated CO_2 selective adsorption for polymer **1**. A bulk gas composition: $CO_2:CH_4=40:60$ (typical composition of biogas) and $CO_2:N_2=10:90$ (typical composition of flue gas), $CO_2:CO=CO_2:O_2 =35:65$.

However, both **1** and **2** can absolutely adsorption CO_2 at 293K, relative to a broad gas like that of N_2, CH_4, O_2, and CO. For polymer **1**, the CO_2 adsorption amount at 1atm is 35cm^3/g, which is almost 5.6 and 19.6 times higher than CH_4 and N_2 uptake (Fig. 5). To estimate the CO_2 adsorption selectivity, we carried out the theory calculation based on the ideal adsorbed solution theory (IAST) and these single-component gas adsorption isotherms.[17] The results were shown in Fig. 6, indicative of higher CO_2 adsorption selectivity over N_2, O_2, and CO. For polymer **2**, the CO_2 adsorption amount (3.9 cm^3/g at 1atm and 293K) is very small, but exceed other gases like that of N_2, CH_4, O_2, and CO, also suggesting selective CO_2 adsorption. But, due to smaller adsorption amount of them, similar theory calculation based on IAST could not get reasonable value. Generally speaking, CO_2 selective adsorption is highly related to two factors such as matching aperture and special adsorption point.[17] Thereby, selective adsorption of CO_2 in **1** is reasonable, as it meet the above criterion in this way that the aperture of 3.5Å in polymer **1** is less than CO_2 diameter of 3.3Å, and extensive, free-standing acylamide groups were observed. But for **2**, the factor of matching aperture is excluded due to framework collapse after activation, and the smaller CO_2 adsorption should be surface adsorption due to the interactions between CO_2 molecule and acylamide groups.

As for polymers **3** and **4**, they exhibited typical type I behavior of N_2 adsorption at 77K, as shown in Fig. 7 and 8, suggesting a Brunauer-Emmett-Teller (BET) surface area of 69.5 m^2/g for **3** and 1382.8 m^2/g for **4**. Single-component gas adsorption isotherms of CO_2, CO, O_2, CH_4 and N_2 were also measured at 293K from 0 to 1 atm. Samples **3** exhibit CO_2 uptake capability of 25.56 cm^3/g at 1 atm, whereas the adsorption of CH_4, CO, N_2 and O_2 were all less than 6.6 cm^3/g at 1 atm. By contrast, samples **4** perform higher CO_2 uptake capability of 43.2 cm^3/g at 1 atm, and the adsorption of CH_4, CO, N_2 and O_2 were all below 12.6 cm^{3}g^{-1} at 1 atm. These results indicate selective adsorption of CO_2 in polymers **3** and **4**. Furthermore, based on these adsorption isotherms, we estimated the selectivities for CO_2/CH_4, CO_2/CO, CO_2/N_2, CO_2/O_2 by using the ideal adsorbed solution theory (IAST). And the results are shown in Fig. 7 and 8. It is clear that polymers **3** show high CO_2 adsorption selectivity over N_2, CO and moderate CO_2 adsorption selectivity over O_2 and CH_4, whereas polymers **4** show high CO_2 adsorption selectivity over N_2, CO, O_2, and moderate CO_2 adsorption selectivity over CH_4. And the results are also comparable with that

observed in some benchmarking MOFs for CO_2 selective adsorption.[18]
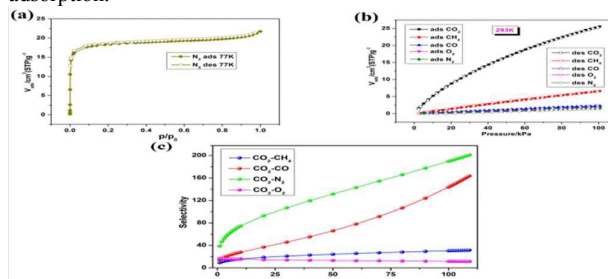
Fig. 7 (a) The N_2 adsorption isotherms of **3** at 77K; (b) Gas adsorption isotherms at 293K; (c) The calculated IAST selectivity of CO_2 over other gases at 293K.A bulk gas composition: $CO_2:CH_4=40:60$ (typical composition of biogas) and $CO_2:N_2=10:90$ (typical composition of flue gas), $CO_2:CO=CO_2:O_2 =35:65$.
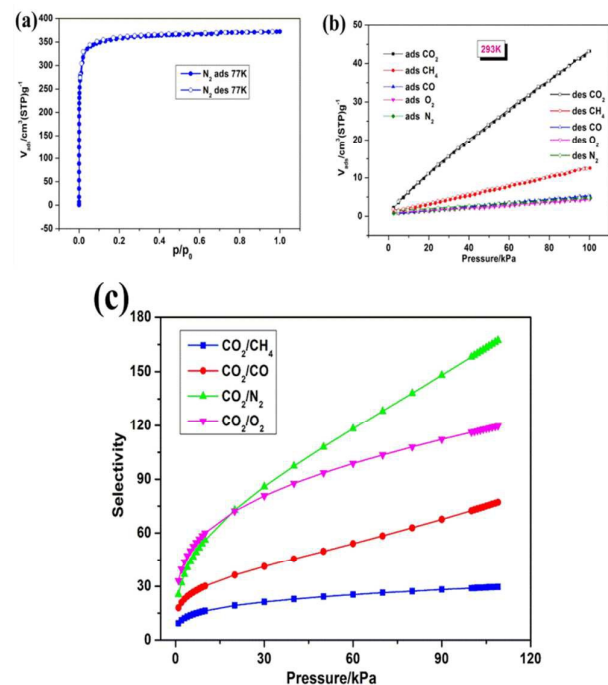
Fig. 8 (a) The N_2 adsorption isotherms of **4** at 77K; (b) Gas adsorption isotherms at 293K; (c) The calculated IAST selectivity of CO_2 over other gases at 293K.A bulk gas composition: $CO_2:CH_4=40:60$ (typical composition of biogas) and $CO_2:N_2=10:90$ (typical composition of flue gas), $CO_2:CO=CO_2:O_2 =35:65$.

Conclusions

In this work, we report the synthesis, structure, and gas adsorption of four new porous MOFs in detail. These MOFs were prepared by means of approach of mixed ligands, viz. azo carboxylate ligand *plus* long acylamide-pyridyl ligand. For polymers **1-2**, we explored the effect of position isomer of acylamide-pyridyl ligand on the finally resulted structure and porosity, and found that this method would be effective to control the interpenetration number of net and consequently porosity. On the other hand, for polymers **3-4**, the effect of amount of solvents on the finally resulted structure and

porosity is investigated, indicating that this method would be facile to generate structure diversity and enhance porosity. Most importantly, all these polymers display various degree of selective adsorption towards CO_2, suggesting potential application in CO_2 capture and separation.

Acknowledgements

Notes and references

1 a) M. O'Keeffe, O. M. Yaghi, *Chem. Rev.* 2012,**112**, 675; b) J. R.Li, J. Sculley, H. C. Zhou, *Chem. Rev.* 2012, **112**, 869.
2 a) S. M. Cohen, *Chem. Rev.* 2012, **112**, 970; b) J. P. Zhang, Y. B. Zhang, J. B. Lin, X. M. Chen, *Chem. Rev.* 2012, **112**, 1001; c) M. Yoon, R. Srirambalaji, K. Kim, *Chem. Rev.* 2012, **112**, 1196; d) C. Wang, T. Zhang, W. B. Lin, *Chem. Rev.* 2012, **112**, 1084.
3 a) Y. J. Cui, Y. F. Yue, G. D. Qian, B. L. Chen, *Chem. Rev.* 2012, **112**, 1126; b) C. A. Kent, D. Liu, T. J. Meyer, W. B. Lin, *J. Am. Chem. Soc.* 2012, **134**, 3991; c) F. Luo, J. L. Chen, L. L. Dang, W. N. Zhou, H. L. Lin, J. Q. Li, S. J. Liu, M. B. Luo, *J. Mater. Chem. A*, 2015, **3**, 9616; d) L. L. Wang, F. Luo, L. L. Dang, J. Q. Li, X. L. Wu, S. J. Liu, M. B. Luo, *J. Mater. Chem. A*, 2015, **3**, 13724; e) F. Luo, C. B. Fan, M. B. Luo, X. L. Wu, Y. Zhu, S. Z. Pu, W. Y. Xu, G. C. Guo, *Angew. Chem. Int. Ed.* 2014, **53**, 9298.
4 a) R. S. Batten, *CrystEngComm* 2001, **3**, 67; b) S. R. Batten, R. Robson, *Angew. Chem., Int. Ed.* 1998, **37**, 1460; c) P. K. Thallapally, J. Tian, M. R. Kishan, C. A. Fernandez, S. J. Dalgarno, P. B. McGrail, J. E. Warren, J. L. Atwood, *J. Am. Chem. Soc.* 2008, **130**, 16842; d) L. Ma, W. Lin, *Angew. Chem., Int. Ed.* 2009, **48**, 3637.
5 O. K. Farha, J. T. Hupp, *Acc. Chem. Res.* 2010,**43**, 1166.
6 a) L. Qin, J. S. Hu, M. D. Zhang, Z. J. Guo, H. G. Zheng, *Chem. Commun.*, **2012**, *48*, 10757; b) J. S. Hu, L. Qin, M. D. Zhang, X. Q. Yao,Y. Z. Li,Z. J. Guo,H. G. Zheng, Z. L. Xue, *Chem. Commun.*, **2012**, *48*, 681.
7 Y. P. Ren, X. J. Kong, L. S. Long, R. B. Huang, L. S. Zheng, *Cryst. Growth Des.*, 2006, **6**, 572.
8 a) M. Eddaoudi, J. Kim, N. Rosi, D. Vodak, J. Wachter, M. O'Keeffe, O. M. Yaghi, *Science* 2002, **295**, 469; b) J. Hafizovic, M. Bjorgen, U. Olsbye, P. D. C. Dietzel, S. Bordiga, C. Prestipino, C. Lamberti, K. P. Lillerud, *J. Am. Chem. Soc.* 2007, **129**, 3612.
9 a) L. Ma, W. Lin, *J. Am. Chem. Soc.*2008, **130**, 13834; b) S. Ma, D. Sun, M. Ambrogio, J. A. Fillinger, S. Parkin, H.-C. Zhou, *J. Am. Chem. Soc.* 2007, **129**, 1858; c) S. Bureekaew, H. Sato, R. Matsuda, S. Yo Kubota, R. Hirose, J. Kim, K. Kato, M. Takata, S. Kitagawa, *Angew. Chem. Int. Ed.* 2010, **49**, 7660.
10 J. J. Zhang, L. Wojtas, R. W. Larsen, M. Eddaoudi, M. J. Zaworotko, *J. Am. Chem. Soc.* 2009, **131**, 17040.
11 H. L. Jiang, Y. Tatsu, Z. H. Lu, Q. Xu, *J. Am. Chem. Soc.* 2010, **132**, 5586.
12 a) O. Shekhah, H. Wang, M. Paradinas, C. Ocal, B. Schupbach, A. Terfort, D.Zacher, R. A. Fischer, C. Woll, *Nat. Mater.*2009, **8**, 481; b) O. Shekhah, H. Wang, S. Kowarik, F. Schreiber, M. Paulus, M. Tolan, C. Sternemann, F. Evers, D. Zacher, R. A. Fischer, C. Woll, *J. Am.Chem. Soc.* 2007, **129**, 15118.
13 O. K. Farha, C. D. Malliakas, M. G. Kanatzidis, J. T. Hupp, *J. Am.Chem. Soc.* 2010, **132**, 950.
14 a) Z. Su, J. Fan, T. Okamura, W. Y. Sun, N. Ueyama, *Crystal Growth & Design*, **2010**, *10*, 3515; b) S. L. Li, K. Tan, Y. Q.Lan, J. S. Qin, M. N. Li, D. Y. Du, H. Y. Zang, Z. M. Su, *Crystal Growth & Design*, **2010**, *10*, 1699; P. Mahata, M.Prabu, S. Natarajan, *Inorg. Chem.* 2008, **47**, 8451.
15 A. L. Spek, *PLATON*, 2001.
16 V. A. Blatov and D. M. Proserpio, TOPOS. Program package for multipurpose crystallochemical analysis, Samara StateUniversity, The Russia, 2008.
17 a) A. L. Myers, J. M. Prausnitz, *AIChE J.* 1965, **11**, 121; b) J. Duan, M. Higuchi, R. Krishna, T. Kiyonaga, Y. Tsutsumi, Y. Sato, Y. Kubota, M. Takata, S. Kitagawa, *Chem. Sci.* 2014, **5**, 660.
18 a) K. Sumida, D. L. Rogow, J. A. Mason, T. M. McDonald, E. D. Bloch, Z. R. Herm, T. Bae, J. R. Long, *Chem. Rev.* 2012, **112**, 724; b) J. R. Li, Y. G. Ma, M. C. McCarthy, J. Sculley, J. M. Yu, H. K. Jeong, P. B. Balbuena, H. C. Zhou, *Coord. Chem. Rev.* 2011, **255**, 1791.

Construction of structural diversity and fine-tuned porosity in acylamide MOFs by synthetical approach

Wan-Ting Yao, Ming-Biao Luo, Xue-Feng Feng*, Pan-Pan Meng, Le-Le Gong, and Feng Luo*
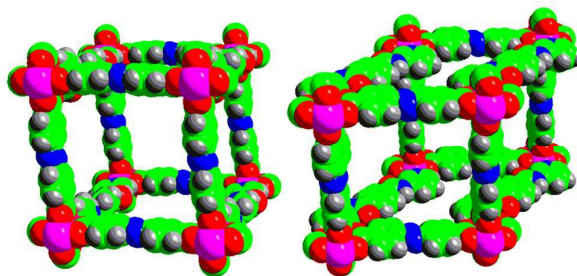
In this work, we explored the effect of position isomer of acylamide-pyridyl ligand on the finally resulted structure and porosity, and the effect of amount of solvents on the finally resulted structure and porosity, resulting in caused significant alteration involving in interpenetration number, enhanced potential porosity, as well as pore configuration.